STUDY ON THE FUEL JET EVOLUTION UNDER TRANS/SUPERCRITICAL CONDITIONS AND DIFFERENT ENVIRONMENT PRESSURE CONDITIONS

*Wu WEI [1], Jin BA [1], Lun ZHAO [*2], Gang XIAO [*2], Maozhao XIE [3]*

[1]School of Mechanical Engineering, Guizhou University, Guiyang 550025, China

[2] Institute of intelligent Manufacturing Techology,Shenzhen Polytechnic, Shenzhen, 518055, China

[3]School of Energy and Power Engineering, Dalian University of Technology, Dalian 116024, China

[*] Corresponding author; E-mail: zhaolun@szpt.edu.cn, xiaosteel@szpt.edu.cn

In Liquid Rocket Engines or Internal Combustion Engines, increasing the inlet fuels temperature or chamber pressure exceeding its critical point is capable of improving the combustion efficiency. Under these conditions, the thermophysical and transport properties have an important effect on fluids mixing and combustion process. In this study, the fuel of n-heptane injected into a multi-species environment are simulated by Large Eddy Simulations and the performance of the injected fuel temperature and different chamber conditions are compared in conjunction with high accuracy equation of state and transport properties. The results show that as the injected temperature or the chamber pressure increase, the penetration length and density gradient decrease, while the width of mixing layer increase. The results obtained in this investigation indicated that for the single injection condition, by increasing the fuel inlet temperature or chamber pressure, the essence is to reduce the initial density ratio, thereby reducing the density stratification between the jet and environment gas, which is beneficial to the jet mixing and combustion process.

Key words*: Large Eddy Simulation; density stratification; supercritical Injection; mixing layer*

1. Introduction

Recently, for the purpose of improving the mixing and combustion effects, the internal combustion engine often operates at pressure that exceeds the critical pressure of injected fuel. Generally, before ignition, the chamber pressure can reach more than 3.0 MPa, while the critical pressure of most hydrocarbon fuel is around 1.5-3.0 MPa, and after ignition, the pressure in the chamber can reach as much as 6.0 MPa. In such conditions, the thermodynamic state will change from subcritical to supercritical state, which plays a key role in the fluid mixing process[1]. Under supercritical environment, attraction between molecules is weakened, and the surface tension almost disappears, leading to a crucial difference in jet disintegration between transcritical and subcritical injection. As a consequence, the classical primary, secondary atomization and evaporation at low pressure conditions do not occur, instead, dense fluid with finger-like structures peels off from the liquid core and mix quickly with environment gas, at which turbulence diffusion has a very important effect on the mixing process[2]. Yang[3] and Bellan[4] performed a comprehensive reviews on

supercritical mixing and combustion. Hence, in order to design high performance combustion devices, further research is needed to understand the fundamental mechanisms of the jet mixing behavior at supercritical conditions.

In the past 30 years, motivated by the liquid rocked engines operating at much high pressure conditions that is above the critical pressure of injected fluids, numerous experimental studies[5-8] was performed on the cryogenic nitrogen or fuel injection under supercritical environment. Results from the shadowgraph images obtained in these investigations confirmed that when the chamber pressure exceeds the injected fluid, the jet surface structure changes drastically. The conventional primary and secondary atomization phenomenon at subcritical environment disappeared at supercritical conditions because of the vanish of surface tension and enthalpy of vaporization. Hence, the jet structure contains liquid-like density and gas-like diffusivity, having a spatial growth rate similar to a variable density gaseous jet[1, 9]. Recently, concerns over energy crisis and environmental pollution issues accelerated research and development on supercritical injection system in diesel engine. Zoldak, Boer et al[10, 11], Dahms and Oefelein[12, 13] and researchers from Engine Combustion Network[14] conducted experimental investigation on various alkane fuels injection into a constant volume chamber filled with nitrogen or air under supercritical environment. In their experiments, the development of conventional breakup and atomization behavior in subcritical condition disappeared, instead, the mixing behavior were considered to be dominated by fluid turbulence flow.

In numerical research, both theoretical and numerical method is an alternative way to further explore the mixing behavior under supercritical injection. As a pioneer, a Direct Numerical Simulation was reported by Bellan et al[15, 16], who model a mixing layer of heptane and nitrogen streams at supercritical conditions. In their simulation, the real-gas thermodynamics and transport properties were included in their density-based flow solvers. Similar investigation was conducted by Tani[17] using a cryogenic nitrogen/nitrogen mixing layer to explore the influence of pseudo critical point on mixing process. Zong and Yang[18] and Zong et al[19, 20] performed a LES on the cryogenic nitrogen injection. Results demonstrated that large density-gradient regions around jet surface play the role of stabilizing the flow fluid by damping the velocity fluctuations normal to the jet surface. Park[21, 22] investigated the influence of both turbulent models and EOS on injection mixing characteristics, and they demonstrated that turbulence model has almost negligible effect on jet evolution, while the type of EOS are crucial on numerical simulation. In the application of internal combustion engines, Oefelein et al[13, 23] conducted many simulations on various alkane fuels injected into a constant-volume chamber filled with single-component or multi-component gas. They suggested that fuels enter the chamber as a compressed liquid, instead of a conventional spray. In addition, in terms of heat transfer[24-28], supercritical fluids are also considered having an important application, hence, the study of supercritical fluids is of great significance.

In the present study, fuel injection into the multi-species supercritical chamber is simulated by LES. This paper focuses on the influence of density-gradient stratification on the jet interface thickness and mixing characteristics.

2. Numerical method

In LES, a spatial filtering operation is performed over the Navier-Stokes equations, which separate small-scale vortexes from large-scale vortexes, and a subgrid scale (SGS) mode is used for

the small-scale vortexes. Hence, the instantaneous mass, momentum, energy and species conservation equations can be expressed as follow

$$\frac{\partial \overline{\rho}}{\partial t} + \frac{\partial (\overline{\rho}\tilde{u}_i)}{\partial x_i} = 0 \tag{1}$$

$$\frac{\partial (\overline{\rho}\tilde{u}_i)}{\partial t} + \frac{\partial (\overline{\rho}\tilde{u}_i\tilde{u}_j + \overline{p}\delta_{ij})}{\partial x_j} = \frac{\partial (\tilde{\tau}_{ij} - \tau_{ij}^{SGS})}{\partial x_j} \tag{2}$$

$$\frac{\partial \overline{\rho}\tilde{e}_t}{\partial t} + \frac{\partial [(\overline{\rho}\tilde{e}_t + \overline{p})\tilde{u}_i]}{\partial x_i} = \frac{\partial [\tilde{u}_j\tilde{\tau}_{ij} + \overline{q}_i - H_i^{SGS} + \sigma_i^{SGS}]}{\partial x_i} \tag{3}$$

$$\frac{\partial \overline{\rho}\overline{Y}_i}{\partial t} + \frac{\partial}{\partial x_j}(\overline{\rho}\overline{Y}_i\overline{u}_j - \overline{\rho}D_{i,m}\frac{\partial \overline{Y}_i}{\partial x_j} + \Phi_{j,m}^{SGS}) = 0 \tag{4}$$

In the above equation, ui, τ ij, Yi, ρ, p, represent the velocity components, viscous stress tensor, species mass fractions, density and pressure, respectively. The total energy et is defined as: . The unclosed term: energy fluxes HiSGS , stresses τ ijSGS， and viscous work σijSGS are derived as follow

$$\tau_{ij}^{SGS} = (\overline{\rho u_i u_j} - \overline{\rho}\tilde{u}_i\tilde{u}_j) \tag{5}$$

$$H_i^{SGS} = (\overline{\rho e_t u_i} - \overline{\rho}\tilde{e}_t\tilde{u}_i) + (\overline{\rho u_i} - \overline{\rho}\tilde{u}_i) \tag{6}$$

$$\sigma_{ij}^{SGS} = (\overline{u_j\tau_{ij}} - \tilde{u}_j\tilde{\tau}_{ij}) \tag{7}$$

$$\Phi_{j,m}^{SGS} = \overline{\rho}(\overline{Y_i u_j} - \overline{Y}_i\overline{u}_j) \tag{8}$$

In equation (5)-(8), the unclosed SGS terms need a model to close. According to Park[21] investigation, comparing to the equation of state, the turbulence model has limit influence on the supercritical condition. Hence, the subcritical turbulence model can be extended to the supercritical regime. In this paper, Smagorinsky model[29] is used and detail information can be found in Lilly[30].

To close the above governing equations, the PR[31] real EOS is applied. For real-gas mixtures, the one-fluid van der Waals[32] mixing rules are imbedded into the code. Based on the EOS, the detail expression of thermodynamic properties are given by Kim[33]. The transport properties are predicted by Chung et al[34] model, while the mass diffusion coefficients are given by using Kinetic Theory[35].
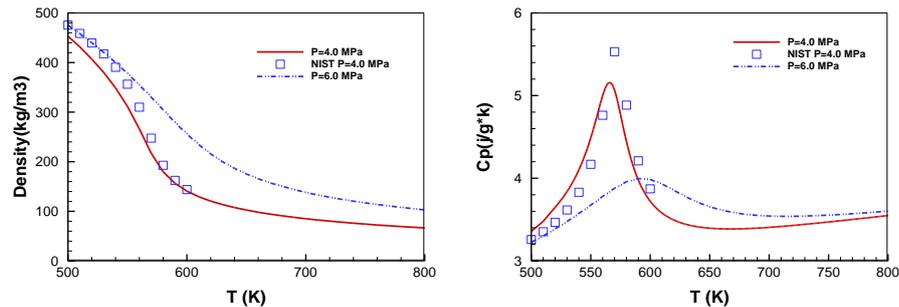

Fig. 1 Density and specific heat prediction by PR EOS

To verify accuracy of the algorithm with Peng-Robinson (PR) equation of state (EOS), the density and specific heat calculated for n-heptane at both 4.0 MPa and 6.0 MPa are presented in Fig.1. For comparison, the (National Institute of Standards and Technology) NIST[36] values at the pressure of 4.0 MPa are also plot in the figure. The density and specific heat profile show good agreement with NIST well except that the specific heat has a relative high deviation as the temperature comes to its pseudo-boiling point. By a close observation, a distinct peak is formed in both pressure conditions, while the crest gradually becomes flat and move to higher temperatures regions with the pressure increasing from 4.0 MPa to 6.0 MPa.

2.1. Numerical scheme validation

For supercritical injection, the real fluid EOS (PR) is crucial and is imbedded into the codes. To verify the accuracy of the algorithm for a multi-species, a methane burner without considering the combustion model is simulated using both ideal gas and PR EOS. The model is symmetrical and the grid system is presented in Fig.2, at which finer grids are applied around the jet center region. An injector with a diameter of 0.01 m is fixed at the center, and the methane with a sustained velocity 80 m/s is injected into the chamber. The accompanied air velocity is 0.5 m/s, flowing from the periphery of the nozzle. Initially, the temperature of the methane and air is 300K, and the pressure is 1 atm. At the right boundary, pressure outlet condition is prescribed. For both cases, the standard κ-ε model is applied, and the density, mass fraction of methane and velocity distribution along the jet flow direction are shown in Fig.3. As we know that when the fluid properties are far from its critical condition, both the real gas EOS (PR) and perfect gas law has the same accuracy in thermodynamic and transport properties prediction. In Fig 3, one can find that the two equations predict almost the same profile, demonstrating that the modified numerical algorithm can reproduce the perfect gas well as the gas is far from its critical temperature. Hence, the algorithm is reliable and can be used to simulate the following n-heptane injection.
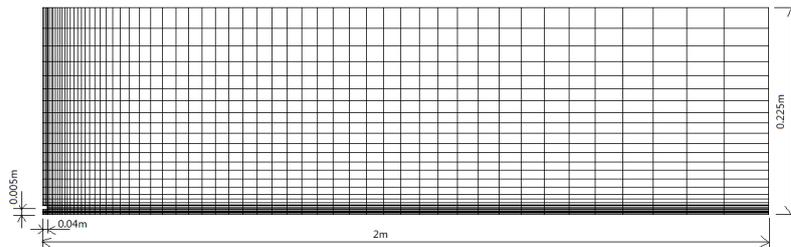

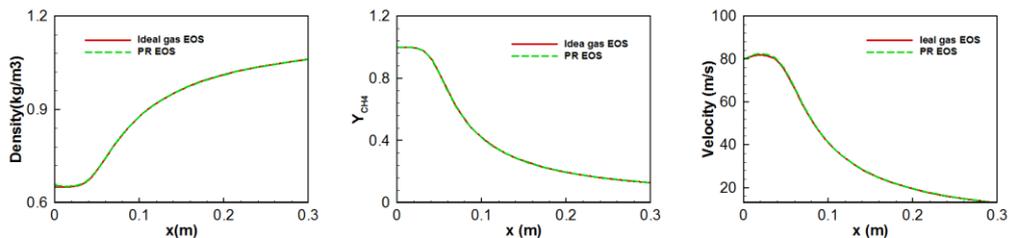**Fig. 2 Model dimensions and grid system of methane burner**

Fig. 3 Comparison of density, mass fraction ch4 and velocity profiles along the axis calculated by two equation of state

4

3. Flow configuration and numerical method

The experimental model of Hossain et al[10] is used to verify the revised program, where n-heptane with initial temperature of 573K was injected into a cylindrical chamber with a mixture of nitrogen, oxygen and water at 4.0 MPa, and the composition of species are shown in table 1. Transcritical/supercritical injection phenomena can be classified into different types according to the state of the injected fuel and the environmental conditions in the cylinder. So far, many scholars generally believe that both the temperature T and pressure P are higher than the critical point corresponding to supercritical injection, while the temperature T is subcritical and the pressure P is supercritical corresponding to subcritical injection. To investigate the pressure effect, we define two transcritical cases with initial injection temperature 520K while the chamber pressure is equal to 4.0 MPa and 6.0 MPa, respectively. In all cases, the jet velocity remains at a constant value of 348 m/s. The initial conditions of the three calculation models are listed in table 2. The experimental model was performed in a cylinder chamber with an injection diameter of 0.15mm at axial direction. In order to save computational resources, the selected computation domain does not strictly follow the test requirements, hence, the calculation cylindrical height and diameter is 55 mm and 20 mm, respectively, which is sufficient to exclude the influence of far-field boundary on jet mixing process. The computation domain is discretized with O-grid type, and mesh is refined around the injector, having a total number of 4.8 million cells.

Table 1. Initial condition in chamber

N_2 (mole fraction)	O_2 (mole fraction)	H_2O (mole fraction)	P_∞ (MPa)	ρ_∞ (kg/m^3)
0.808	0.064	0.128	4.0	16.64

Table 2. The parameters of simulation condition

Case	T_{inj}[K]	u_{inj}[m/s]	T_∞[K]	p[MPa]	ρ_{inj}/ρ_∞	Re_{inj}
1	573	348	770	4.0	13.7	432800
2	520	348	770	4.0	26.4	334200
3	520	348	770	6.0	18.8	314293

In this study, the above filtered N-S equations are solved using finite volume method. Under high pressure conditions, thermodynamic non-idealities and transport anomalies bring some trouble to numerical methods. According to Park[21], the real EOS is embedded into PISO algorithm, which can be capable of dealing with supercritical fluids. In LES, the convective and viscous terms are discretized using second order scheme, while a second order implicit scheme is applied for temporal terms. For purpose of improving calculation efficiency, a multi-block domain splitting technology with MPI is used for parallel computation.

4. Results and discussion

4.1. Numerical scheme validation

Figure 4 plots the penetration length based on n-heptane distribution for three cases, and compare with experiment values conducted by Hossain et al [10]. Penetration depth is defined as the maximum axial distance at which the mass fraction of n-heptane dropped to 1%. In comparison with experimental data, the trend of simulation result follows the experiment well, yet there are still some deviations. This can be attributed to measurement become very difficult under high pressure and temperature. As can be seen in the figure, the length depth shortened as the pressure increase from 4MPa to 6MPa due to the large density ratio has the effects of stabilizing the jet flow.
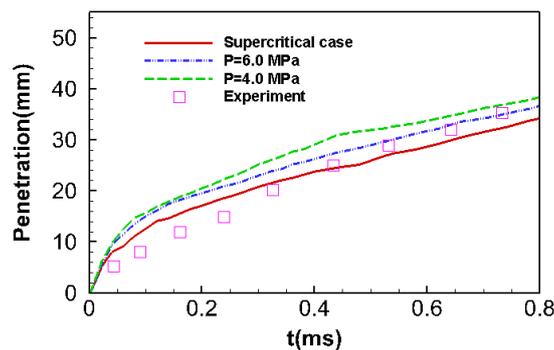
Fig. 4 Penetration of heptane distribution of measured and simulation for three cases
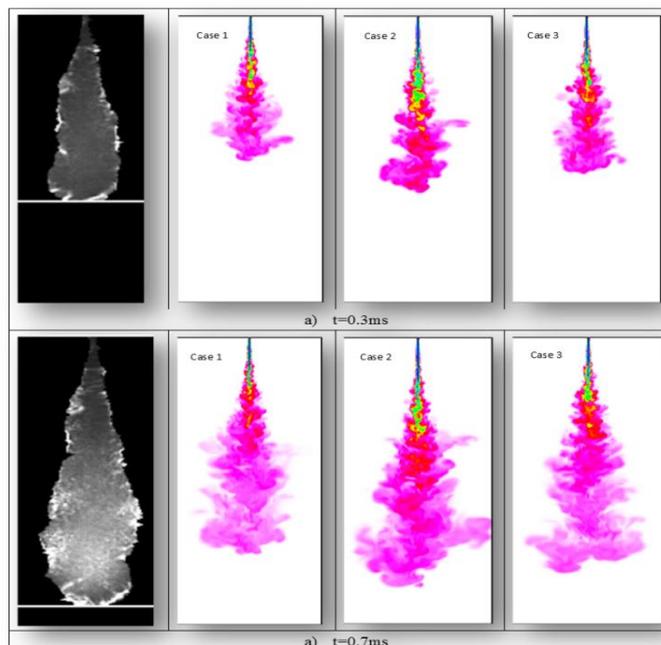

Fig. 5 Simulation contours and Experimental plume based on mass-fraction distribution

Figure 5 presents the contours of n-heptane mass-fraction for three cases and the visual graph obtained by Hossain et al[10] for case 1 at 0.3 ms and 0.7 ms. It is found that numerical simulation can better capture the shape characteristics of the jet. Comparing case 1 and case 2, the interface is more susceptible to disturbances and scroll up in case 1, suggesting that the supercritical case 1 is capable of improving mixing rate. For this reason, the potential core is longer in case 2 owing to the large density

ratio prevent the jet flow from developing radially. While in case 2 and case 3, the vortexes are more easily formed around jet surface as the chamber pressure increase, resulting in a more fast mixing behavior between jet and surrounding gas. Hence, the jet transit deep downstream and forming a longer penetration depth in case 2.
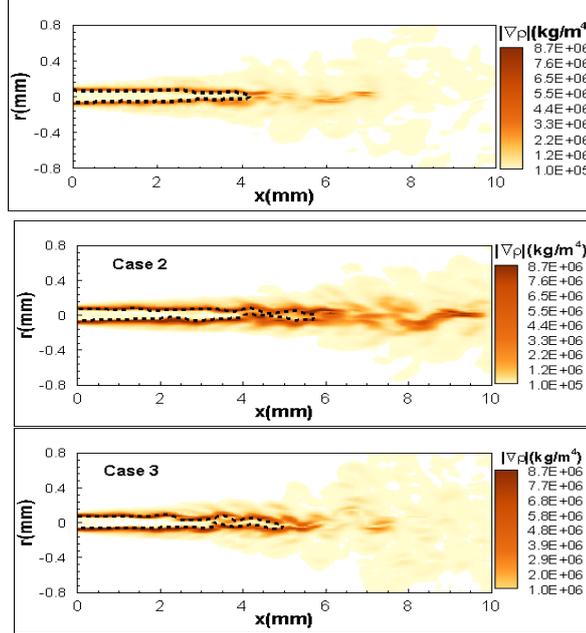

Fig. 6 The density-gradient distribution for case 1(top), case 2(middle) and case 3(bottom). The black dash lines denote the potential core

Figure 6 shows snapshots of density-gradient fields in a plane parallel to the inflow direction for three cases. The black dash refers the minimum value inside the jet core and represent the potential core and jet breakup region. It can be found that large eddy simulation can reproduce the contour characteristics of the jet well. In case 2, where the initial injection temperature is below its pseudo-boiling temperature and sharp density gradients form around the jet surface and the maximum density gradients are much higher than that in the supercritical case 1. These large density gradients hinder the Kelvin-Helmholtz vortex formation and therefore the jet break-up process is delayed. Therefore, in the transcritical case 2, many dense liquid split from the jet surface concentrate at the end of potential core, dissolving gradually into environment gases. While this phenomenon is invisible for the supercritical case 1, where coherent vortex structure develop rapidly close to the injector, and a much faster break-up process. Due to this break-up feature, the length potential core shows a shorter value in case 1 than case 2. Case 2 and case 3 has the same initial conditions except the chamber pressure. By comparing the density gradient distribution in both cases, we have two findings. First, the lower pressure case 2 shows larger density gradient around the jet surface and dense pockets of injected fuel tend to eject from the end of potential core, developing further downstream. Second, the length of potential core shortens in case 3 as the pressure increases.

4.2. Numerical scheme validation

To further study the mixing characteristics of supercritical jet, the transient flow field characteristics are extracted from the flow field at a certain time interval for averaging operation. Figure 7 gives the normalized density(($\rho^* = (\bar{\rho} - \rho_\infty)/(\rho_{in} - \rho_\infty)$)) and compression factor distribution along axial direction. One can notice that the density distributions are unchanging in the

potential core area, and then a rapid decline at the end of potential core occur. In contrast, it is found that the transcritical case 2 has longer potential core, yet a rapid decline at the end for both case 1 and case 3. This can be contributed to the large initial density stratification, which has the effects of delaying the breakup process. For the compression factor, the transcritical case 2 and 3 exhibit larger departures from a perfect gas before the flow are fully developed. In addition, as the pressure increase in case 3, the injected fluid tends to move to the perfect gas direction. When the injected fluid deviates a perfect gas property, more energy is mainly consumed in fluid heating, resulting in a delay for the jet breakup. The mean n-heptane fractions and root-mean-square n-heptane along the axial direction are plotted in Fig. 8. Again, due to the delay effects, the injected n-heptane develops far downstream in case 2, which is similar to the density distribution. For the root-mean-square n-heptane profile, all cases have similar profile with a very small initial district, then sharply increases to the maximum and gradually decreases. Similarly, the supercritical case 1 shows a smaller value after the end of potential core area, followed by the transcritical case 2 and case 1. This is because the large initial density stratification between fluid jet and surrounding gas, leading to a delay on the jet breakup. Due to the breakup behavior, the velocity and turbulent kinetic along the axial direction have similar distribution, which is shown in Fig. 9.
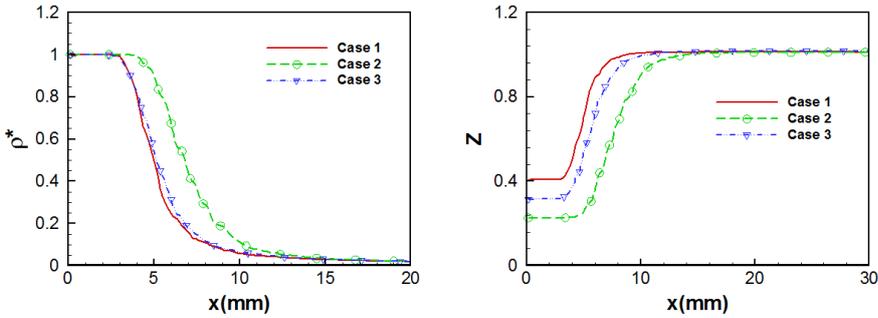

Fig. 7 The normalized density and compression factor distribution at the axis direction
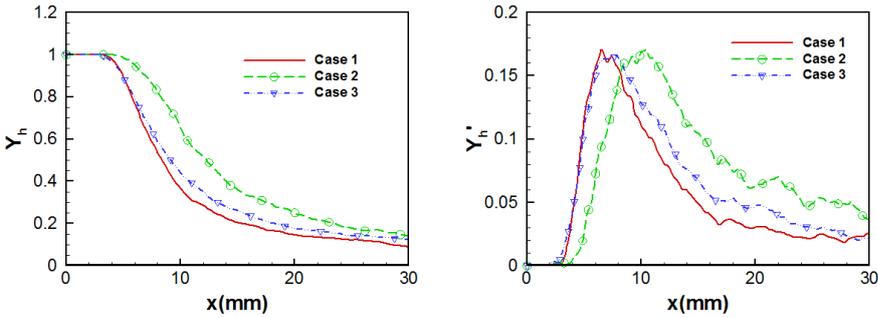

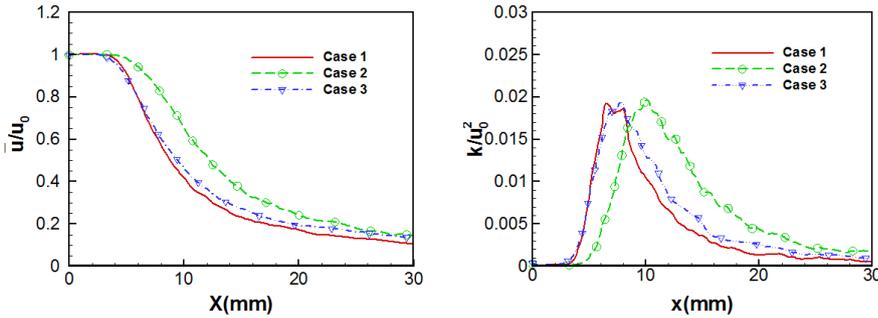**Fig. 8 The mean n-heptane fraction and root-mean-square n-heptane distribution at the jet centerline**
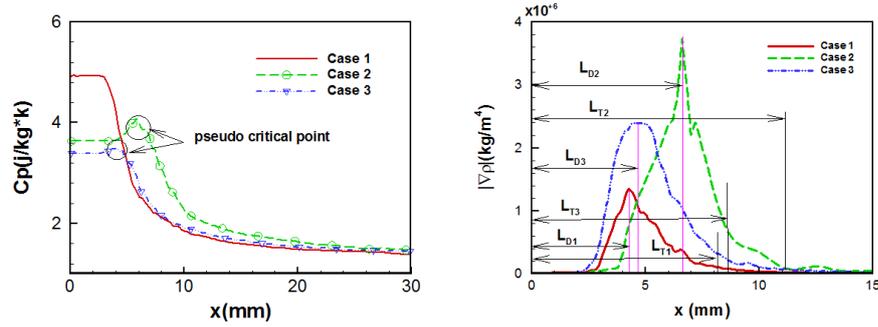

8

Fig. 10 Mean specific heat and density-gradient distribution at the jet centerline

Fig.10 shows the specific heat and density-gradient along the axial direction. For the specific heat profiles, it keeps unchanging, then decrease smoothly in the supercritical case 1. However, this is different from the transcritical case 2 and 3, where a maximum peak value is visible at the end of potential core area. While the max value is downsized comparing to case 2 and 3, for the environment gas penetrate into the jet and change its critical properties. Hence, the multi-species injection is different from that in single species regime, where the dissolution effects play a very important role on fluid heat transfer and dynamic characteristics. Comparing case 2 and 3, the pseudo critical properties is much more suppressed in case 3 as the pressure increase, indicating that increasing the chamber pressure, the pseudo critical properties is more suppressed, which has the effects of promoting the mixing process. In order to understand jet breakup feature, the density-gradient profile along the axis is also plotted in Fig.10, and the jet is divided into three parts: the dense core LD at which the density-gradient reaches its maximum; the transitional region LT where the density-gradient reaches a constant region and after that come to a self-similar region. The dense core LD and transitional region LT are also marked in Fig.10 for three cases. Comparing to supercritical injection, one can recognize that the length of dense core (LD) and transition region (LT) in the transcritical injection shows much higher value, indicating that the supercritical jet is easier to mix with the ambient gas and reach a self-similar area. By comparing the transcritical case 2 and 3, we can find that the jet breakup earlier as the surrounding pressure increase, forming longer dense core (LD) and transition region (LT) in case 3. The most important reason for this phenomenon is the density stratification effect, which is much larger in case 2, followed by case 3 and case 1.

The radial density, n-heptane fraction, specific heat and velocity at x=12mm are plotted in Fig11. One can find that these properties have analogous distribution, where maximum values appear in the axial center and larger value can be found in transcritical case2 near its center area. However, when the fluid jets develop away from the center area, these properties show larger values in supercritical case 1. It means that n-heptane develops deeper to radial area, which facilitates the mixing of fuel injection with sounding gas.
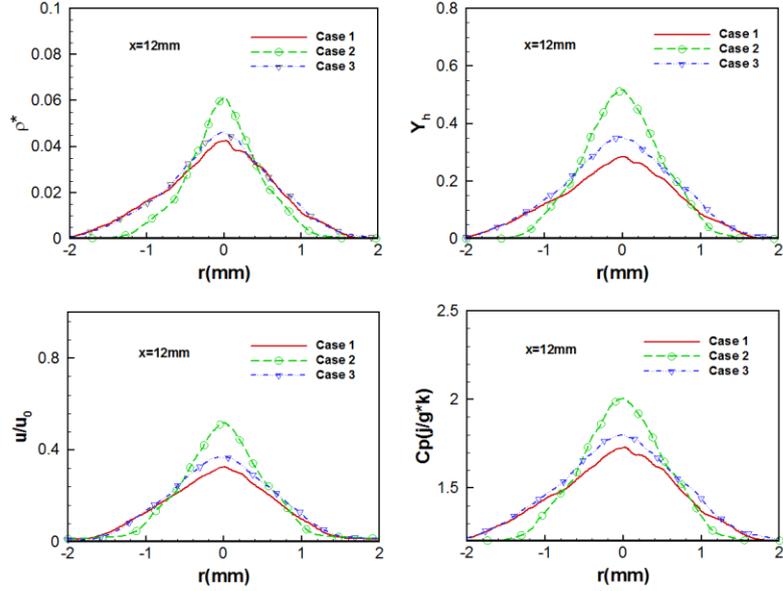
Fig. 11 The density, n-heptane mass fraction, specific heat and velocity profile along radial at x=12mm
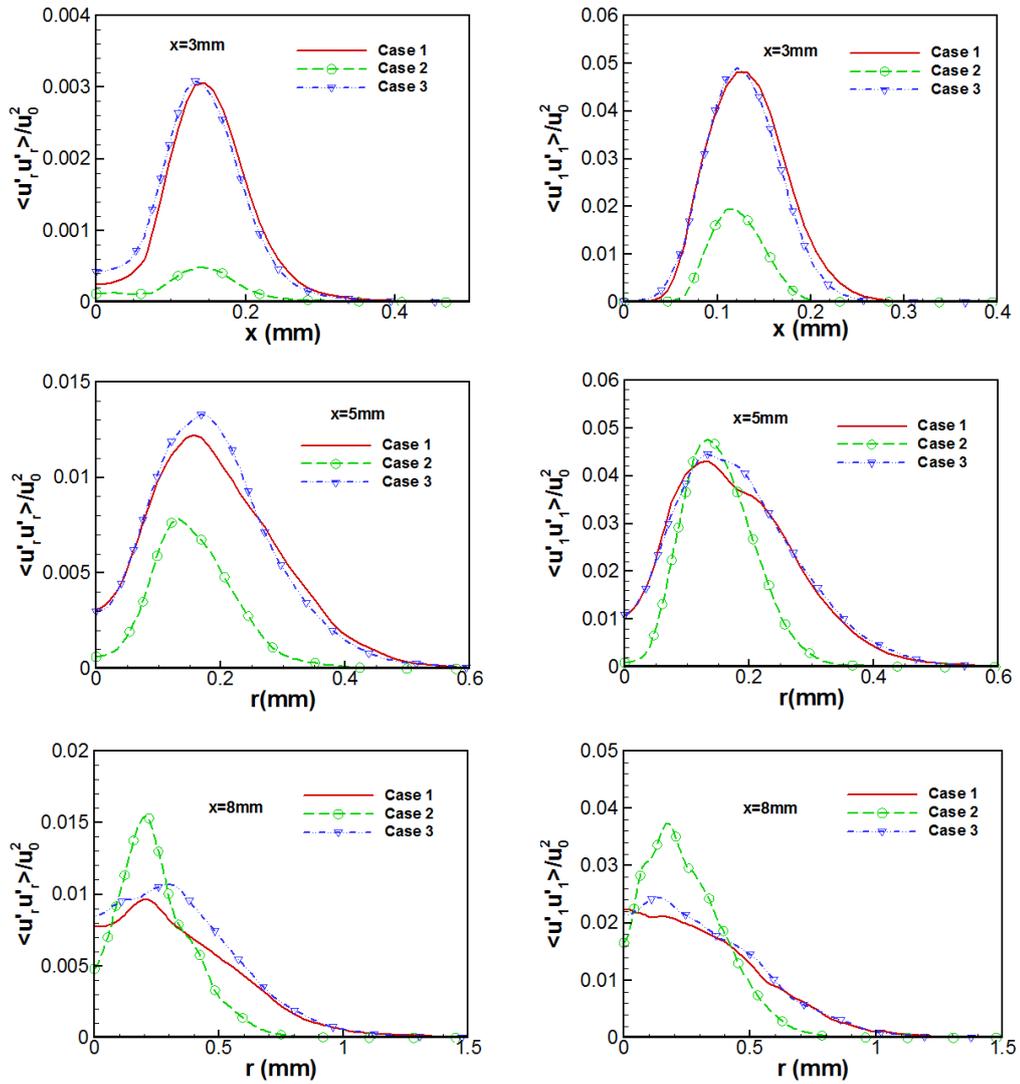

Fig. 12 Comparison of Reynolds stresses in radial and axial at x/D=3, 5, 8 for three cases

To investigate the influence of breakup feature on fluid jet dynamics, the Reynolds stresses in axial and radial for three cases are analyzed and are plotted at Fig.12. At x/D=3, both the axial and radial fluctuations have a maximum value around the jet outside, and It is obvious that the peaks are relatively wide and larger for case1 and case3 due to smaller density stratification. As the jet develop further downstream, the peak values of axial and radial fluctuations are captured, indicating that turbulence energy propagates from axial to radial area by mean of vortices formation and breakup on the jet surface. By a close inspection, it is visible that the maximum values move to higher r/D regions, yet the span are widened and flattened as the jet break up. This phenomenon is delayed in the transcritical case 2 for the jet's surface is stabilized for the initial higher density stratification and large heat capacity (shown in Fig.10), where much more energy is needed as the jet transit across its pseudo-critical temperature.
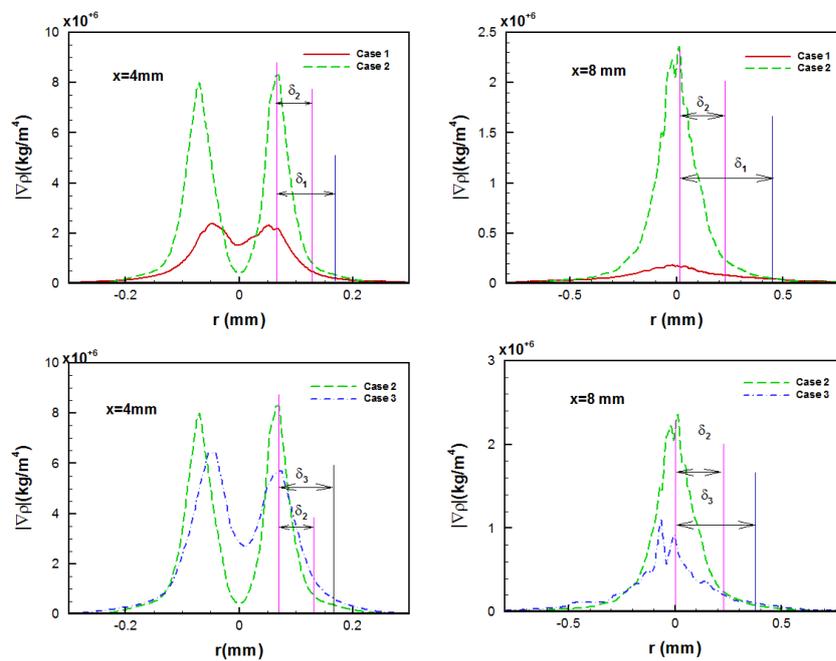

Fig13. Radial density gradient profile at x=4mm and x=8mm for three cases

Table3. Mixed layer thickness value for three cases

x coordinate	Case1(mm)	Case2(mm)	Case3(mm)
4mm	0.212	0.056	0.11mm
8mm	0.456	0.112	0.38mm

In turbulent mixing dominated flow, the density gradients are significant important on the jet mixing behavior. The radial density gradient distributions at x=4mm and x=8mm for three cases are presented in Fig13. Firstly, in the potential core area at x=4mm, the jet surface is surrounded by large density gradient and the transcritical case2 has a larger value, which is consistent with the cloud diagram in Fig 6. As the jet fluids develop downstream (x=8mm), the density gradient decrease gradually. The transcritical case 3 shows similar trend with a lower density distribution as the chamber pressure increase. To quantify the jet-gas interface characteristics, a mixing layer thickness (MLT) δ is

defined as the distance from the maximum $|\nabla\rho|_{max}$ to the point at which its value decreases to $0.1|\nabla\rho|_{max}$ in axial center position. According to this definition, the MLT δ for three cases are marked in Fig 13, and its values are given in table 3. It is obvious that the MLT in supercritical case1 shows much larger value than the transcritical case2 and the ratio of their value is about 2 in x=4mm and 4 in x=8mm, respectively, while the MLT become wider as the environment pressure increased. By comparison the three operation conditions, we can come to the conclusion that whether it is increasing the injection temperature or the ambient pressure, the essence is to reduce the density stratification, which is beneficial to the mixing effect of the jet and the ambient gas.

5. Results and discussion

In this investigation, the PISO algorithm is appropriately modified to be able to handle the real-gas fluid, a methane burner model is applied to validate the algorithm. The thermophysical and transport properties are modeled and added into the program as well, and the behavior of turbulence jet mixing is studied by LES in supercritical conditions.

As the injected temperature increase to supercritical, or the chamber pressure increase, the mixing process strengthened. Thus the penetration length shortened and vortex are relatively easy to form on the jet surface. By analyzing the density gradient, the transcritical injections form a much larger value around the jet surface and a longer potential core region, besides, the density gradient value decrease by increasing the environment pressure. By defining the mixing layer with density gradient distribution, we find that the supercritical case forms a thicker value and the mixing layer became thicker as the chamber pressure increase. The thicker mixing layer means a better mixing effect. The mean velocity, density distribution and turbulence characteristics come to a similar conclusion. Through research, we find that the radio of the initial density ratio between the injected fluid with chamber pressure play an relative important role on the jet mixing process. Therefore, whether it is by increasing the fuel inlet temperature to supercritical or increasing the pressure in the combustion chamber, its essence is to reduce the initial density radio between the injected fuel and the chamber, which helps to improve the mixing effects. In the future, a systematic investigation on the influence of density stratification on supercritical mixing behavior is of great significance.

References

[1] Gerber, V., *et al.*, Fluid injection with supercritical reservoir conditions: Overview on morphology and mixing, *The Journal of Supercritical Fluids*, *169* (2021), pp. 1-22

[2] Lagarza-Cortés, C., *et al.*, Large-eddy simulation of transcritical and supercritical jets immersed in a quiescent environment, *Physics of Fluids*, *31* (2019), 2, pp. 1-14

[3] Yang, V., Modeling of supercritical vaporization, mixing, and combustion processes in liquid-fueled propulsion systems, *Proceedings of the Combustion Institute*, *28* (2000), 1, pp. 925-942

[4] Bellan, J., Supercritical (and subcritical) fluid behavior and modeling: drops, streams, shear and mixing layers, jets and sprays, *Progress in Energy & Combustion Science*, *26* (2000), 4, pp. 329-366

[5] Branam, R., Mayer, W., Characterization of Cryogenic Injection at Supercritical Pressure, *Journal of Propulsion & Power*, *19* (2003), 3, pp. 342-355

[6] Oschwald, M., Micci, M., Spreading Angle and Centerline Variation of Density of Supercritical Nitrogen Jets, *Atomization & Sprays*, *12* (2002), 1-3 pp. 91-106

[7] Candel, S., *et al.*, Experimental Investigation of Shear Coaxial Cryogenic Jet Flames, *Journal of Propulsion & Power*, *14* (1998), 5, pp. 826-834

[8] Shin, B., *et al.*, Effects of supercritical environment on hydrocarbon-fuel injection, *Journal of Thermal Science*, *26* (2017), 2, pp. 183-191

[9] Magalhães, L. B., *et al.*, Computational study on coaxial nitrogen-hydrogen injection at supercritical conditions, *AIAA SCITECH 2022 Forum*, 2022, pp. 1-12.

[10] Hossain, K., *et al.*, Transonic Combustion: Model Development and Validation in the Context of a Pressure Chamber, *Sae Technical Papers*, 2012

[11] Boer, C. D., *et al.*, Transonic Combustion - A Novel Injection-Ignition System for Improved Gasoline Engine Efficiency, *SAE 2010 Powertrains Fuels & Lubricants Meeting*, 2010.

[12] Dahms, R. N., Oefelein, J. C., On the transition between two-phase and single-phase interface dynamics in multicomponent fluids at supercritical pressures, *Physics of Fluids*, *25* (2013), 9, pp. 092-103

[13] Dahms, R. N., *et al.*, Understanding high-pressure gas-liquid interface phenomena in Diesel engines, *Proceedings of the Combustion Institute*, *34* (2013), 1, pp. 1667-1675

[14] ECN. Engine Combustion Network. http://www.sandia.gov/ecn/.

[15] Miller, R. S., *et al.*, Direct numerical simulations of supercritical fluid mixing layers applied to heptane–nitrogen, *Journal of Fluid Mechanics*, *436* (2001), 4, pp. 1-39

[16] Okong'O, N. A., Bellan, J., Direct numerical simulation of a transitional supercritical binary mixing layer: Heptane and nitrogen, *Journal of Fluid Mechanics*, *464* (2002), 10, pp. 1-34

[17] Tani, H., *et al.*, A Numerical Study on a Temporal Mixing Layer under Transcritical Conditions, *Computers & Fluids*, *85* (2013), 85, pp. 93-104

[18] Zong, N., Yang, V., An efficient preconditioning scheme for real-fluid mixtures using primitive pressure-temperature variables, *International Journal of Computational Fluid Dynamics*, *21* (2007), 5, pp. 217-230

[19] Yang, V., Cryogenic fluid jets and mixing layers in transcritical and supercritical environments, *Combustion Science & Technology*, *178* (2006), 1, pp. 193-227

[20] Zong, N., *et al.*, A numerical study of cryogenic fluid injection and mixing under supercritical conditions, *Physics of Fluids*, *16* (2004), 12, pp. 4248-4261

[21] Park, T. S., LES and RANS simulations of cryogenic liquid nitrogen jets, *Journal of Supercritical Fluids*, *72* (2012), 12, pp. 232–247

[22] Park, T. S., Kim, S. K., A Pressure-Based Algorithm for Gaseous Hydrogen/Liquid Oxygen Jet Flame at Supercritical Pressure, *Numerical Heat Transfer Part A Applications*, *67* (2015), 5, pp. 547-570

[23] Oefelein, J. C., *et al.*, Detailed Modeling and Simulation of High-Pressure Fuel Injection Processes in Diesel Engines, *Sae International Journal of Engines*, *5* (2012), 3, pp. 1410-1419

[24] Gopal, J. M., *et al.*, Understanding Sub and Supercritical Cryogenic Fluid Dynamics in Conditions Relevant to Novel Ultra Low Emission Engines, *Energies*, *13* (2020), 12, pp. 30-38

[25] Yang, Z., *et al.*, Reynolds-Averaged Navier-Stokes Equations Describing Turbulent Flow and Heat Transfer Behavior for Supercritical Fluid, *Journal of Thermal Sciences*, *30* (2021), 1, pp. 191-200

[26] Mohseni, M., Bazargan, M., Entropy generation in turbulent mixed convection heat transfer to highly variable property pipe flow of supercritical fluids, *Energy Conversion and Management*, *87*(2014), 87,pp. 552–558

[27] Bai, W., Xu, X., Comparative analyses of two improved CO2 CCHP systems driven by solar energy, *Thermal Science*, *22* (2018), 2, pp. 693-700

[28] Sarkar, J., Improving thermal performance of microchannel electronic heat sink using supercritical CO2 as coolant, *Thermal Science*, *23* (2017), 1, pp. 243-253

[29] Smagorinsky, J., General circulation experiments with the primitive equations, *Monthly Weather Review*, *91* (1963), 3, pp. 99-164

[30] Lilly, D. K., A proposed modification of the Germano subgrid‐scale closure method, *Physics of Fluids A Fluid Dynamics*, *4* (1992), 4, pp. 633-635

[31] Prausnitz, J. M., *et al.*, *Molecular thermodynamics of fluid-phase equilibria*, Prentice-Hall, 1969.

[32] Redlich, O., Kwong, J. N., On the thermodynamics of solutions; an equation of state; fugacities of gaseous solutions, *Chemical Reviews*, *44* (1949), 1, pp. 233-244

[33] Kim, T., Kim, Y., Kim, S. K., Numerical study of cryogenic liquid nitrogen jets at supercritical pressures, *Journal of Supercritical Fluids*, *56* (2011), 2, pp. 152-163

[34] Chung, T. H, *et al.*, Generalized multiparameter correlation for nonpolar and polar fluid transport properties, *Industrial & Engineering Chemistry Research*, *27* (1988), 27, pp. 671-679

[35] Reid, R. C., *et al.*, *The properties of gases and liquids*. McGraw-Hill, 1977

[36] http://webbook.nist.gov/chemistry/fluid